NUPEC BFBT SUBCHANNEL VOID DISTRIBUTION ANALYSIS USING THE MATRA AND MARS CODES

DAE-HYUN HWANG*, JAE JUN JEONG and BUB DONG CHUNG
Korea Atomic Energy Research Institute
1045 Daedeok-daero Yuseong-gu, Daejeon, Korea
*Corresponding author. E-mail : dhhwang@kaeri.re.kr

Received June 27, 2008
Accepted for Publication November 24, 2008

The subchannel grade void distributions in the NUPEC (Nuclear Power Engineering Corporation) BFBT (BWR Full-Size Fine-Mesh Bundle Tests) facility were evaluated with the subchannel analysis code MATRA and the system code MARS. Fifteen test series from five different test bundles were selected for an analysis of the steady-state subchannel void distributions. Two transient cases, a turbine trip without a bypass as a typical power transient and a re-circulation pump trip as a flow transient, were also chosen for this analysis. It was found that the steady-state void distributions calculated by both the MATRA and MARS codes coincided well with the measured data in the range of thermodynamic qualities from 5 % to 25 %. The results of the transient calculations were also similar and were highly feasible. However, the computational aspects of the two codes were clearly different.

KEYWORDS : Subchannel Flow Mixing, Void Distributions in a Rod Bundle, MATRA, MARS, BFBT Data

1. INTRODUCTION

Subchannel analysis codes [1,2] are of vital importance for the thermal-hydraulics of nuclear reactor cores. KAERI (Korea Atomic Energy Research Institute) developed a subchannel analysis code termed MATRA [3] on the basis of the COBRA-IV-I code [1] to analyze the thermal hydraulic characteristics in rod bundles for several types of nuclear reactors, including pressurized water reactors (PWR) [4], liquid metal cooled reactors [5], and gas cooled reactors [6]. The MATRA code was systematically assessed using various test data against a wide range of flow conditions, including the critical heat flux (CHF) data base for rod bundles [7]. At the same time, KAERI developed a thermal-hydraulic system code termed MARS [8] for a more realistic simulation of nuclear reactor systems. The MARS code is based on a consolidated version of the one-dimensional system code RELAP5/MOD3 and the three-dimensional (3D) reactor vessel thermal-hydraulics code COBRA-TF [9]. As the COBRA-TF code has subchannel analysis capability, the MARS code can be utilized for a subchannel analysis as well as a system analysis. However, assessment of the COBRA-TF code has mainly focused on reflood heat transfers and, recently, its subchannel flow mixing model [10] has been improved and assessed against some well-known experimental data, including the ISPRA 16-rod tests [11], the GE 9-rod tests [12], and the two interconnected subchannel tests [13].

Given that both the MATRA code and the MARS 3D module were originally developed for the analysis of a PWR core, they have mainly been used in subcooled or low-quality conditions. In the adverse operating conditions near a CHF, however, a PWR core can experience a higher void fraction at a subchannel, which may occur due to a lower pressure and mass velocity in the reactor core. Moreover, some advanced light water reactors may be operated at low velocity conditions. Thus, it is necessary to validate them for higher void fraction conditions to improve their CHF prediction capability and to extend the applicable range of these codes to advanced light water reactors.

The OECD NEA has organized the NUPEC BFBT Benchmark Program [14] not only for comparisons of currently available computational approaches but also to encourage the development of novel next-generation approaches that focus on processes that are more microscopic. The NUPEC 8x8 rod bundle test facility has a full range of steady-state test capabilities under typical BWR operating conditions and can simulate the unsteady characteristics of operational transients. Void distributions were measured for a fine-mesh using an X-ray computerized tomography (CT) scanner at a point 50 mm above the heated zone for steady-state cases. The attained spatial resolution was as small as 0.3 mm $\times$ 0.3 mm, which is very valuable for the assessment of both subchannel codes and computational fluid dynamics codes. In addition, three

X-ray densitometers (DM) were used to measure the cross-sectional average void fractions during transients at three different axial locations. In the framework of the OECD/NRC BFBT Benchmark Program, subchannel grade benchmark exercises were established. These include fifteen steady-state void distributions tests and two transient tests.

In this study, subchannel grade benchmark exercises are examined using the MATRA and MARS codes for assessment purposes and a comparative investigation. The effects of the fuel assembly type, radial and axial power distribution, and the inlet flow condition are investigated. Key differences of the two codes are discussed in terms of their physical models for subchannel flow mixing. The computational aspects of the two codes are also discussed.

2. SUBCHANNEL FLOW MODELS OF THE MATRA AND MARS CODES

In general, the accuracy of a subchannel flow analysis is strongly dependent on the modeling of the flow mixing between adjacent subchannels. However, this subchannel mixing phenomena are quite complicated and difficult to decompose into elementary exchange terms. They are normally decomposed arbitrarily into three components [15]: (i) A diversion crossflow that occurs due to imposed transverse pressure gradients, (ii) Turbulent mixing that occurs due to stochastic pressure and flow fluctuations, and (iii) "Void drift" that occurs due to the strong tendency of the vapor phase to drift towards the higher velocity regions. These three components are generally considered to be independent and are written in a rational manner in conservation equations.

The key features of the MATRA and MARS codes are compared in Table 1. As explained in Table 1, the MARS code is a system code capable of a subchannel analysis, whereas the MATRA is a subchannel analysis code. Each code has its own advantages for a subchannel analysis. Thus, users should select the appropriate code to take advantage of these codes according to the problem type. In the following subsections, the subchannel flow models of the two codes are described.

2.1 The MATRA Code

MATRA is a subchannel analysis code that adopts mixture transport equations for two-phase flow conditions. The continuity, energy, and axial/lateral momentum equations for an arbitrary subchannel i are expressed as follows:

Continuity:

$$A_i \frac{\partial \rho_{m,i}}{\partial t} + \frac{\partial \dot{m}_i}{\partial z} + \sum_j w_{ij} + \sum_j w'_{i \leftrightarrow j} = 0 . \quad (1)$$

Table 1. Comparison of the Key Features of the MATRA and MARS Codes

Feature	MATRA	MARS
Code category	Subchannel analysis code	System analysis code
Fluid model	Mixture model	Two-fluid model
Subchannel flow mixing model	Equal-mass-exchange model or equal-volume-exchange void drift model.	Equal-volume-exchange void drift model.
Numerical scheme	Fully-implicit scheme; the time step is not limited by the material Courant limit.	Semi-implicit scheme; the time step is limited by the material Courant limit.
Steady-state calculation	Very efficient; using a very large time step, a steady-state state is reached in a time-step advancement.	Not efficient; to reach a steady state, a null-transient advancement is needed, which requires a somewhat long computing time.
Boundary conditions	The flow conditions at the inlet and exit of the core are needed.	The flow conditions at the inlet and exit of the core may be given. A simultaneous calculation of the system and core thermal-hydraulics is also possible.
Strength and weakness	Very efficient and user-friendly for a subchannel analysis. However, it is assumed that the axial flow is dominant in the reactor core. Thus, the convergence is not guaranteed when the transverse flow is strong.	Not user-friendly for a subchannel analysis. Instead, a coupled calculation feature of "system thermal-hydraulics, 3D reactor kinetics, and subchannel analysis" is feasible [16].

Energy:

$$A_i \frac{\partial}{\partial t}\rho_{m,i}h_{m,i} + \frac{\partial}{\partial z}\left(\dot{m}_i \bar{h}_i\right) + \sum_j w_{ij}\hat{h}^* + \sum_j w'_{ij}\left(h_i - h_j\right) = Q. \quad (2)$$

Axial momentum:

$$\frac{\partial \dot{m}_i}{\partial t} + \frac{\partial}{\partial z}\left(\frac{\dot{m}_i^2 v'}{A_i}\right) + \sum_j w_{ij}u^* + f_T \sum_j w'_{ij}\left(u_i - u_j\right) = -\bar{A}\frac{\partial P}{\partial z} - F_z. \quad (3)$$

Lateral momentum:

$$\frac{\partial w_{ij}}{\partial t} + \frac{\partial}{\partial z}\left(w_{ij}\bar{u}_i\right) + \frac{1}{l}\sum_j w_{ij}\bar{v}_i = \frac{s_{ij}}{l}\left(P_i - P_j\right) - F_{ij}. \quad (4)$$

The source terms in the above equations are expressed as

$$Q = \frac{\partial}{\partial z}\left(k_i \frac{\partial T_i}{\partial z}A_i\right) - \sum_j \frac{k_j s_{ij}}{l}\left(T_i - T_j\right) + \sum_n \xi_n \langle q''_n \rangle, \quad (5)$$

$$F_z = \frac{1}{2}\left\{\frac{f\phi^2}{d_{h_i}\rho_m} + \frac{K}{\rho' \Delta x}\right\}_i \frac{\dot{m}_i^2}{A_i} + A_i \rho_{m,i} g\cos\theta, \quad (6)$$

$$F_{ij} = \frac{1}{2}K_{ij}\frac{w_{ij}|w_{ij}|}{\rho^* s_{ij} l} + s_{ij}\rho_{m,i} g\sin\theta \quad (7)$$

The last term of the left side of conservation equations (1), (2) and (3) represents the net exchange of the mass, energy, and axial momentum due to the turbulent mixing between subchannel i and its surrounding subchannels. By introducing a turbulent mixing parameter, β, which is defined as the ratio of the lateral fluctuating mass flux to the axial mass flux of the fluid in the subchannel, the turbulent mixing flow rate per unit length from subchannel i to j is expressed as

$$w'_{ij} = \beta \cdot s_{ij} \cdot G_{avg}. \quad (8)$$

The turbulent mixing parameter is normally determined from a thermal mixing test under single-phase conditions. The two-phase mixing phenomenon is still not perfectly understood; it is formulated to be identical to the single-phase mixing model in the COBRA-IV-I code. The turbulent mixing model employed in the COBRA-IV-I code is based on the equal-mass-exchange (EM) concept. In the EM model, it is assumed that the fluctuating mass flow rates between the interacting subchannels are identical. Thus, there is no net mass transfer due to turbulent mixing, and a diversion crossflow is the only mechanism that transfers a mass between the subchannels.

In two-phase flow conditions, however, a substantial amount of mass transfer has been observed experimentally, as has energy and momentum transfers [17]. To explain this behavior, a model was devised that considers an equal-volume exchange of two-phase mixture globs between subchannels assuming that the net two-phase turbulent mixing was proportional to a non-equilibrium void fraction gradient [15]. The equal-volume-exchange and void-drift (EVVD) model was incorporated into the MATRA code. The net fluctuating mass velocity from channel i to channel j is expressed as

$$w'_{i\leftrightarrow j} \equiv w'_{ij} - w'_{ji} = \left(w'_{ij}\right)_{SP} \cdot \theta \cdot \left[\left(\alpha_j - \alpha_i\right) - K_{VD}\frac{\left(G_j - G_i\right)}{G_{avg}}\right], \quad (9)$$

where $(w'_{ij})_{SP}$ is the turbulent mixing flow rate per unit length under single-phase conditions, and θ is a two-phase multiplier for the turbulent mixing rate [20]. A detailed description of the correlation parameters is available in the literature [18]. The first term in the bracket represents an equal volume exchange due to the turbulent mixing between subchannels. If the void fraction in channel j is larger than that in channel i, the first term has a positive value and reduces the void fraction at channel j. The second term reveals an equilibrium void distribution that results in void drift phenomena. This void drift phenomenon is characterized by a strong tendency toward an equilibrium void distribution. In other words, the vapor has a strong affinity for a subchannel with a larger cross-sectional area and a higher velocity. From this hypothesis, this term has the effect of moving the void towards a higher velocity channel.

Two different models for the void drift coefficient K_{VD} are available in MATRA. The first is a constant K_{VD} model (K_{VD} =1.4), which has been introduced into the THERMIT code [2]. The other is a flow regime dependent model which was derived from an assessment of experimental data [18]. According to this model, the void drift coefficient is expressed as

$$K_{VD} = a_1\left(\frac{\chi - \chi_{OSV}}{\chi_C - \chi_{OSV}}\right) \text{ at a bubbly-slug flow regime } (\chi_{OSV} \le \chi < \chi_C), \quad (10)$$

$$K_{VD} = a_1 + a_2\left(\frac{\chi - \chi_{OSV}}{\chi_C - \chi_{OSV}} - 1\right) \text{ at an annular flow regime } (\chi \ge \chi_C). \quad (11)$$

The models for the slug-annular transition quality, χ_C, and the quality at the onset of a significant void, χ_{OSV}, were selected from an assessment of the experimental data [18]. The quality, χ, in Eqs. (10) and (11) was calculated

from the mean enthalpy of two interacting subchannels. The void drift coefficient becomes zero when χ is lower than χ_{OSV}. The coefficient, a_1, is given as a function of the pressure, and a_2 is a constant [18].

To obtain numerical solutions for the aforementioned equations, an implicit solution scheme in the MATRA code was employed. A fully implicit backward differencing scheme is used for discretization of the governing equations, whereas an upwind differencing is exclusively used for the convective terms. The major variables, including the axial flow, crossflow, enthalpy, pressure and density, are calculated simultaneously for all subchannels through an external iterative sweep of the computational mesh from the bottom of the channel. The solution is considered to be converged when the maximum changes in the crossflow, axial flow and enthalpy satisfy the convergence criteria simultaneously. The boundary conditions imposed on this problem are a specified inlet flow and enthalpy distribution along with a zero inlet crossflow and uniform pressure at the exit of the bundle.

2.2 The MARS Code

The MARS code is a best-estimate thermal-hydraulics system code that is based on a consolidated version of the RELAP5/MOD3 and COBRA-TF codes [8]. The COBRA-TF code was adapted as a three-dimensional thermal-hydraulic module in the MARS code. It uses a two-fluid, three-field model for two-phase flows on rectangular Cartesian or subchannel coordinates and has a subchannel flow mixing model. All of these features of COBRA-TF have been conserved well in the MARS 3-D module. Thus, the MARS code can be utilized for a subchannel analysis.

The governing equations for the two-fluid, three-field model in the MARS 3D module are given below:

Continuity equations:

$$\frac{\partial}{\partial t}(\alpha_k\rho_k)+\nabla\cdot(\alpha_k\rho_k\vec{u}_k)=\Gamma_k \tag{12}$$

where k=l, v, e, and n for a continuous liquid, vapor, entrained liquid, and noncondensible gases, respectively.

Momentum equations:

$$\frac{\partial}{\partial t}(\alpha_k\rho_k\vec{u}_k)+\nabla\cdot(\alpha_k\rho_k\vec{u}_k\vec{u}_k)=\alpha_k\rho_k\vec{g}-\alpha_k\nabla P+\nabla\cdot[\alpha_k(\vec{\tau}_k+\vec{T}_k^T)]+\overline{M}_k^\Gamma+\overline{M}_k^d \tag{13}$$

where k=l, v+n, and e for a continuous liquid, gaseous phase, and entrained liquid, respectively. It is assumed that the vapor and noncondensible gases are in mechanical equilibrium. The interfacial drag and the virtual mass force are included in the last term in Eq(13).

Energy equations:

$$\frac{\partial}{\partial t}(\alpha_k\rho_k h_k)+\nabla\cdot(\alpha_k\rho_k h_k\vec{u}_k)=-\nabla\cdot[\alpha_k(\vec{Q}_k+\vec{q}_k^T)]+\Gamma_k h_k^j+q_{ik}^{''}+\alpha_k\frac{\partial P}{\partial t} \tag{14}$$

where k=l+e, and v+n for a liquid and gaseous phase, respectively. It is assumed that the vapor and noncondensible gases are in thermal equilibrium. In addition, the continuous and entrained liquid fields are assumed to be in thermal equilibrium.

To obtain the numerical solutions, a semi-implicit scheme is used [8]. The diversion crossflow is obtained by solving the transverse momentum equations. It should be noted that, the MARS 3-D module, there are no differences in finding the solution of the axial and transverse momentum equations. For the turbulent mixing and void drift, a simple model is employed. It is based on the work of Lahey [15] and Kelly [19]. The model is similar to that in the MATRA code. However, because the MARS 3D module uses a two-fluid, three-field model for two-phase flows, the model should be modified appropriately. The net mass flux of the vapor phase from subchannel i to j due to a turbulent mixing and void drift is represented in the MARS 3D module as

$$w_{g,i-j}^{''}=\left(\frac{\varepsilon}{l}\right)_{1\varphi}\theta\left\{(\alpha\rho)_{g,i}-(\alpha\rho)_{g,j}-K_{VD}\frac{G_i-G_j}{G_{avg}}\rho_{g,avg}\right\}, \tag{15}$$

where $(\varepsilon/l)_{1\varphi}$ is the turbulent velocity at a single-phase condition [15] and θ is a two-phase multiplier for the turbulent velocity [10, 18]. The void drift coefficient K_{VD} was originally given as an input parameter but was modified later as a function of the pressure. K_{VD} is zero when the void fraction at the donor subchannel (low mass velocity subchannel) is zero. Similarly, the net mass flux of the liquid phase from subchannels i to j due to a turbulent mixing and void drift is

$$w_{l,i-j}^{''}=\left(\frac{\varepsilon}{l}\right)_{1\varphi}\theta\left\{(\alpha\rho)_{l,i}-(\alpha\rho)_{l,j}+K_{VD}\frac{G_i-G_j}{G_{avg}}\rho_{l,avg}\right\}. \tag{16}$$

In Eq. (15), it is assumed that the fluctuating lateral velocity components for the vapor and liquid phases are equal. The mixing model is not applied for the entrained-liquid phase in the MARS 3D module. Equations (15) and (16) are taken into account in the continuity equations for the vapor phase and the continuous liquid phase, respectively. In addition, energy and momentum exchange terms due to the turbulent mixing and void drift are taken into account in the governing equations.

The performance of the subchannel mixing model in the MARS 3D module was examined using well-known rod bundle test data. To cover a wide range of test conditions, the ISPRA 16-rod tests [11], the GE 9-rod tests [12], and the two interconnected subchannel tests [13] were used. These tests were performed under pressures of 16 MPa, 6.9 MPa, and 0.14 MPa, respectively. From the results of the assessment, an optimum void drift coefficient was derived as a function of the system pressure [10]:

$$K_{VD} = 0.112 + 16.4e^{-0.329P} \quad (17)$$

where P is the pressure in MPa. Equation (17) is recommended for a steam-water system under a pressure range between ~6.9 MPa and ~16 MPa.

3. DESCRIPTION OF THE BFBT FACILITY AND BENCHMARK PROBLEMS

The NUPEC 8x8 rod bundle test facility [14] has a full range of steady-state test capabilities under typical BWR operating conditions. It can also simulate the unsteady characteristics of operational transients. Figure 1 shows a schematic of the test facility. A full-scale BWR simulated fuel assembly of an 8x8 rod bundle was installed in the test facility. The heated length of the rod bundle was 3.708 m. Seven spacer grids were used to support the fuel rods in the bundle. The outer diameter of a fuel rod was 12.3 mm, and the rod pitch was 16.2 mm.

Two types of void distribution measurement systems, an X-ray CT scanner and an X-ray densitometer, were used [14]. Void distributions were measured in the fine mesh using the X-ray CT scanner at a point 50 mm above the heated zone for steady-state cases. To avoid the effect of two-phase flow fluctuations, the collection of the projection data was repeated and the results were time-averaged. The attained spatial resolution was as small as 0.3 mm × 0.3 mm. Three X-ray densitometers (DM) were used to measure the cross-sectional average void fractions during the transients, which were located at the axial locations of 0.682 m, 1.706 m, and 2.730 m above the bottom of the heated section. The accuracy of the subchannel void fraction as measured by X-ray CT scanner was estimated to be 3% [14].

Different types of fuel assembly designs with different combinations of their geometries and power shapes were tested during steady-state void distribution experiments. The fuel assembly types are depicted in Fig. 2. Test assembly Type 0 has uniform radial and axial power distributions. Three sub-types of test bundle 0, specifically 0-1, 0-2, and 0-3, were used to evaluate the effects of the radial power distribution on the void fraction distribution by varying the number of unheated rods among them. Test assembly Types 1, 2, and 3 are similar to assembly Type 0-1 with two unheated rods but with different axial heated lengths and different axial power shapes. Assembly Type 4 has a uniform axial power profile only for void distribution measurements.

The subchannel-wise steady-state void distributions in the simulated BWR fuel assemblies were provided for the benchmark. The benchmark exercise covered fifteen test series from five different test bundles that included a different number of unheated rods and radial/axial power

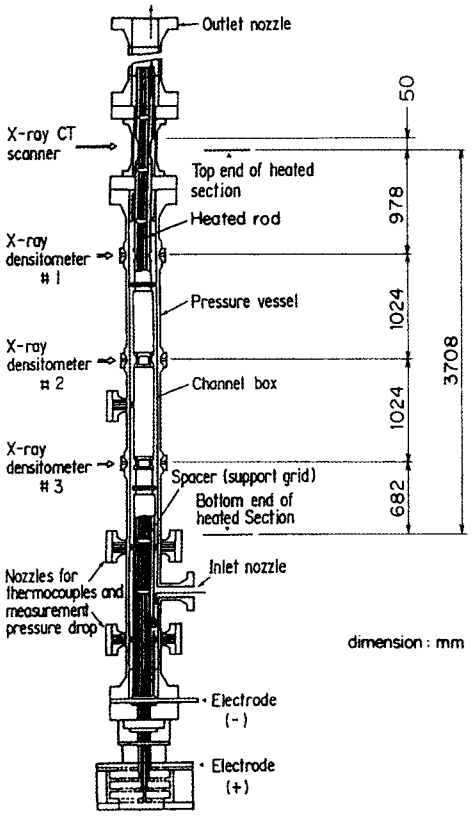

Fig. 1. The Schematic of the NUPEC BFBT Facility [14]

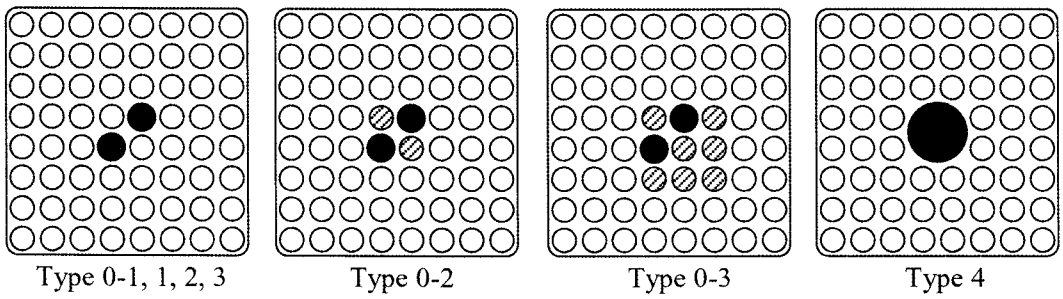

Fig. 2. Fuel Assembly Types; the Black Color Denotes a Water Rod, and the Shaded Area Denotes an Unheated Rod (The Diameters of the Water Rods are 15 mm in Types 0 ~ 3 and 34 mm in Type 4)

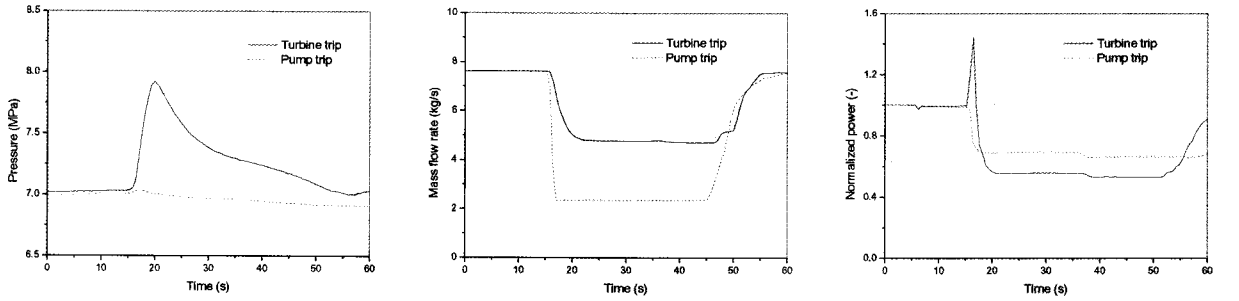

(a) Exit pressure vs. time (b) Inlet mass flow rate vs. time (c) Normalized power vs. time

Fig. 3. Transient Boundary Conditions for the Turbine Trip and the Pump Trip

Table 2. Experimental Conditions for the Steady-state Void Distribution Benchmark

Test no.	Assembly type	Pressure (MPa)	Flow rate (t/h)	Inlet subcooling (kJ/kg)	Outlet quality (%)	Power (MW)
0011-55	0-1	7.180	54.03	52.6	5.0	1.90
0011-58	0-1	7.172	54.90	51.0	12.0	3.51
0011-61	0-1	7.210	54.79	50.9	25.0	6.44
0021-16	0-2	7.190	54.85	54.0	5.0	1.91
0021-18	0-2	7.171	54.90	59.8	12.0	3.51
0021-21	0-2	7.179	54.90	51.4	25.0	6.45
0031-16	0-3	7.180	54.96	52.4	5.0	1.92
0031-18	0-3	7.179	54.79	50.0	12.0	3.52
0031-21	0-3	7.171	54.90	49.4	25.0	6.45
1071-55	1	7.191	54.61	52.8	5.0	1.92
1071-58	1	7.158	55.07	50.3	12.0	3.52
1071-61	1	7.200	54.65	51.8	25.0	6.48
4101-55	4	7.195	54.59	52.9	5.0	1.92
4101-58	4	7.152	54.58	50.6	12.0	3.52
4101-61	4	7.180	54.65	52.5	25.0	6.48

distributions [14]. Experimental conditions for the steady-state void distribution benchmark are summarized in Table 2.

Two transient cases, a turbine trip without a bypass as a typical power transient and a re-circulation pump trip as a flow transient, were also chosen for this benchmark exercise. Assembly Type 4 was used in the transient cases [14]. The boundary conditions for the two transients are illustrated in Fig. 3. The cross-sectional averaged void fractions were measured at four different axial levels with two types of detectors, as explained earlier. As the X-ray densitometer measurements were taken from a beam passing through the centerline of a subchannel, it overestimated the subchannel void fractions, especially at the upper part of the bundle.

4. THE RESULTS OF THE MATRA AND MARS CALCULATIONS

4.1 Analysis Methods

The calculation parameters and correlations of the MATRA code for the analysis of the BFBT benchmark exercises are summarized in Table 3. The test section was modeled using all subchannels with 72 uniform axial meshes for the steady-state and 140 non-uniform axial meshes for the transient exercises. The numbering of the subchannels for the MATRA calculations is provided in Fig. 4. The overall trend of the void distribution was also evaluated for the test bundles by grouping the subchannels into five zones, as shown in Fig. 4.

For the MARS input model, which is shown in Fig. 5,

1/2 or 1/4 radial symmetry assumptions depending on the bundle geometry and radial power distributions were used for computational efficiency. As the MARS 3D module does not have a steady-state calculation option, a null transient calculation is required to reach a steady state. This requires a somewhat long computation time. 24 equal-length axial meshes were used for the heated region.

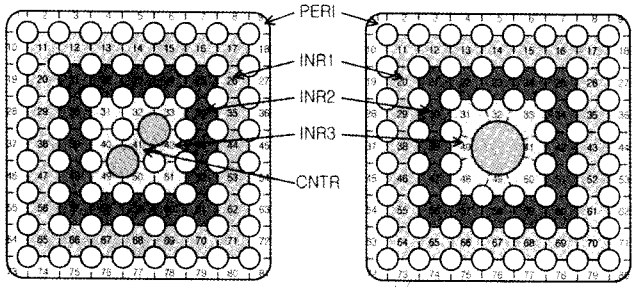

Fig. 4. Subchannel Nodalization of the Test Bundles for the MATRA Analysis

4.2 Steady-State Void Distribution Problems

From the viewpoint of a subchannel grade, it was assumed that the subchannel void distribution depends on the vapor generation rate inside the subchannels and the vapor movement between the subchannels. The vapor generation rate is directly related to the thermal load of the channel (i.e., the channel power divided by the channel flow rate), which is affected by the rod power distribution and the hydraulic characteristics of the subchannels. It is also influenced significantly by the turbulent energy mixing, which is considered to be proportional to the mass velocity in the channel. The vapor movement is explained reasonably by a void drift model that is based on the assumption that the equilibrium void distribution is directly proportional to the velocity distribution of the fluid mixture. Thus, the thermal load and the fluid velocity are important parameters that dominate the subchannel void distribution.

The subchannel void distributions calculated by the MATRA and MARS codes are compared with the BFBT measured data in Fig. 6. The subchannel numbers in Fig.

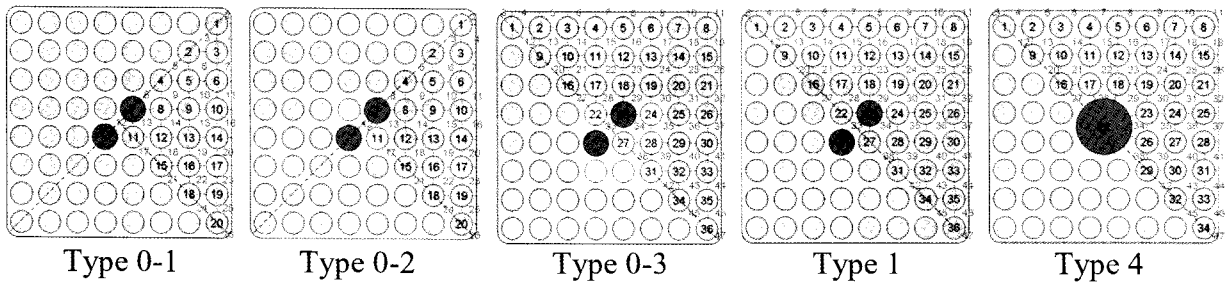

Fig. 5. The MARS Input Model: Channel and Rod Numbers are Given

Table 3. MATRA Models for the BFBT Test Data Analysis

Parameters	Values
Two-phase models	
Field equations	Homogeneous mixture
Subcooled boiling void fraction	Levy model
Bulk boiling void fraction	Modified Armand model
Two-phase friction multiplier	Armand model
Subchannel interaction models	
Crossflow resistance factor	0.5
Turbulent mixing parameter for single-phase	0.005
Two-phase turbulent mixing model	EVVD model (K_{VD} by eqs. 10 & 11)
Hydraulic Resistance Models	
Bundle friction factor	$0.184\ Re^{-0.2}$
Spacer grid loss factor	1.2

6 correspond to those in Fig. 4. In Type 0-1, which has uniform axial and radial power distributions, the hydraulic characteristics of each subchannel dominate the flow distribution inside the bundle. The corner channel revealed a higher thermal load due to a smaller flow area, whereas it revealed a lower mass velocity due to a smaller hydraulic diameter in comparison with the neighboring side channels. The void fraction at a corner channel was found to be lower than the side-channels due to the void drift model that enforced a void migration from a lower-velocity corner channel to a higher-velocity side channel. This tendency was observed in the experimental data for all of the test bundles and was predicted reasonably well by the MATRA and MARS codes, as shown in Fig. 6.

The effect of unheated rods was evaluated by employing three different rod bundles (Types 0-1, 0-2, and 0-3) that

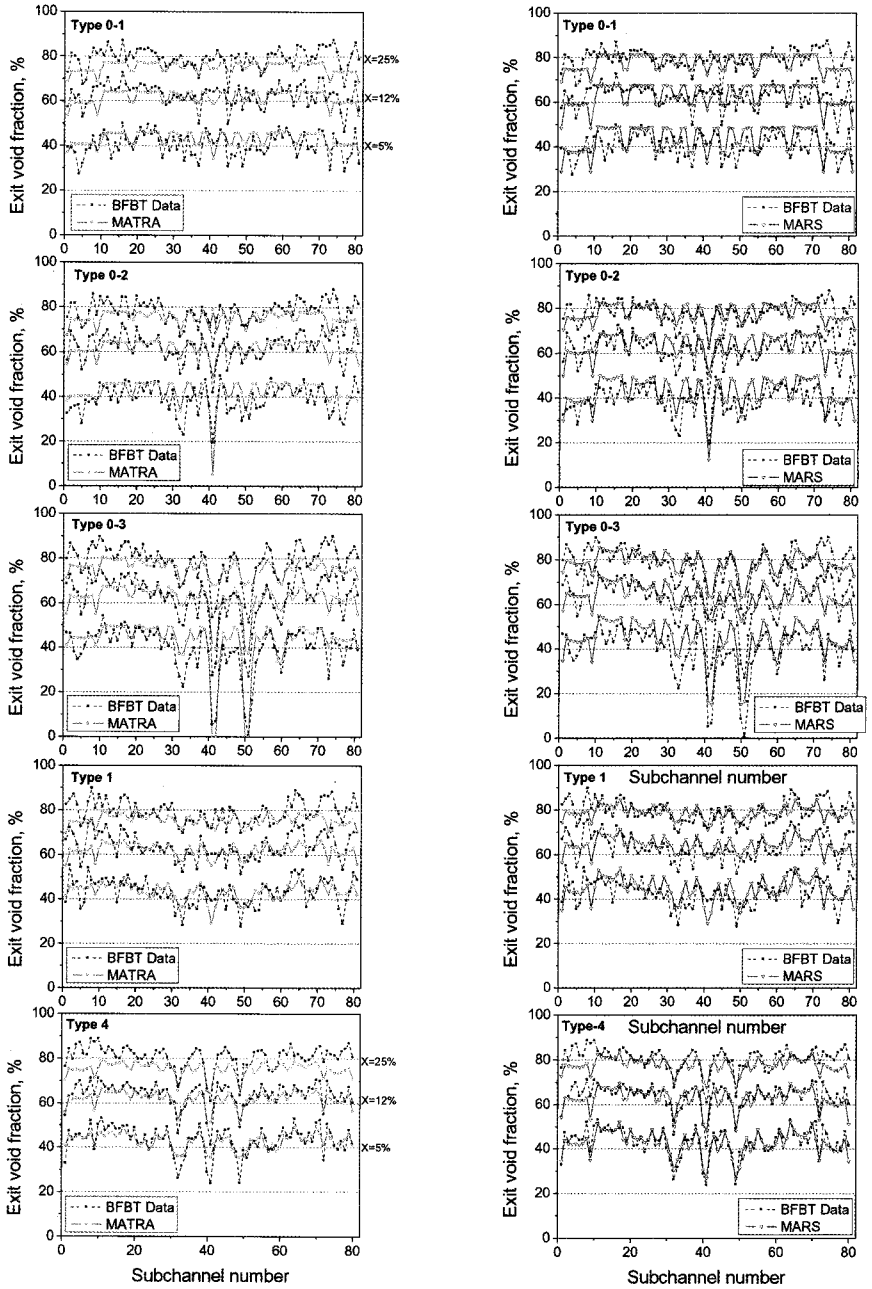

Fig. 6. Comparison of the Subchannel Void Distributions for the BFBT Test Bundles (The Subchannel Numbers in Fig. 4 were Used in the above Figures)

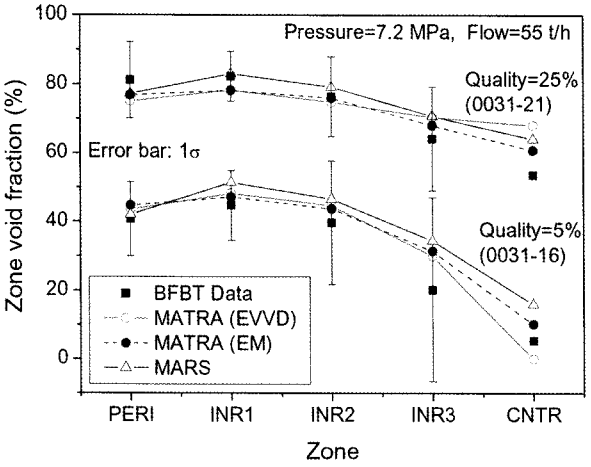

Fig. 7. Comparison of Zone-averaged Void Fractions for Type 0-3 with Four Unheated Rods

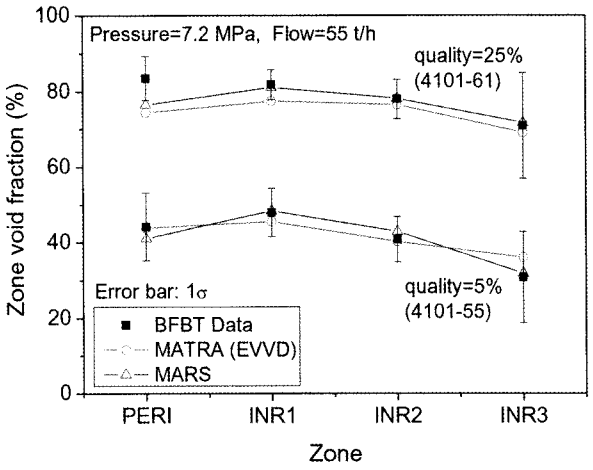

Fig. 8. Comparison of Zone-Averaged Void Fractions for Type 4 with a Central Unheated Rod

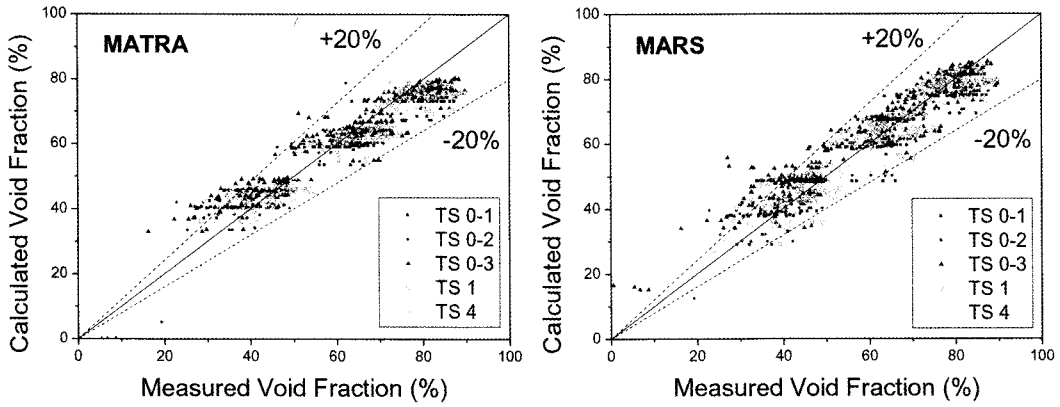

(a) The results of MATRA (b) The results of MARS

Fig. 9. Comparison of Predicted and Measured Subchannel Void Fractions

contained different numbers of unheated rods. As the subchannel at the CNTR region (CNTR channel) consisted of unheated rods, as shown in Figs. 2 and 4, a void could appear in this region via the following two mechanisms. The first of these is a turbulent exchange of the fluid with neighboring channels, which may result in a net transfer of the mass and energy from the cold CNTR channel to the surrounding hot channels; since, a mass reduction is more significant than an energy reduction at the CNTR channel, the resultant turbulent exchange could increase the specific energy at the CNTR channel. The second involves void drift phenomena that may cause a void migration toward a higher velocity channel at the CNTR region.

The analysis results for Type 0-3, which has nine unheated rods in the central region, showed that the MATRA code tended to under-predict the void fraction at the CNTR region at a lower exit quality condition, whereas it over-predicted the CNTR void at a higher quality condition, as shown in Fig. 7. The error bars in this figure represents $\pm\sigma$ (i.e., the standard deviation) of the void fractions for the subchannels, which belong to the same zone. At a lower quality condition, a net increase of the specific energy at the CNTR channel caused by the turbulent mixing was not sufficient to increase the fluid enthalpy up to a saturated condition. Additionally, the void drift was not significant, as the void drift coefficient was determined from the mean enthalpy of two interacting channels. Thus, the void fraction was calculated as zero due to the thermal equilibrium assumption for a mixture in the MATRA code. The void was calculated to appear at the CNTR channel by the MARS code, which adopted two-fluid non-equilibrium models, as shown in Fig. 7.

At a higher quality condition, the CNTR exit condition reached a saturated state due to a sufficient exchange of the mass and energy with neighboring channels. The velocity gradient between the CNTR channel and

Table 4. Summary of the (P-M) Statistics for Phase-I Exercise-1

Type	N_H[1]	Radial/Axial Power Shape	Spacer type	Statistics of subchannel void fraction (P-M)[3], %			
				MATRA		MARS	
				Mean	Std. dev.	Mean	Std. dev.
0-1	62	U / U[2]	Grid	-0.9	5.4	0.7	5.6
0-2	60	U / U	Grid	-0.3	5.7	1.4	5.6
0-3	55	U / U	Grid	-0.2	6.5	2.1	6.8
1	62	NU / NU	Grid	-1.9	5.3	0.4	5.4
4	60	NU / U	Ferrule	-2.6	4.2	-1.5	3.9
All data				-1.2	5.5	0.6	5.7

1) Number of heater rods in the test bundle
2) U: Uniform, NU: Nonuniform
3) P: Predicted void fraction at each subchannel (in %), M: Measured void fraction at each subchannel (in %)

neighboring channels becomes larger as the quality increases. This is attributed to the increase of two-phase pressure losses in the neighboring hot channels. The void drift model in the MATRA and MARS codes revealed an over-estimation for the void inflow to the CNTR channel in comparison with the experimental data.

When the void drift phenomenon was neglected by employing an EM model, a more accurate result was obtained at the CNTR channel for this specific case, as shown in Fig. 7. However, a lower void fraction at the corner channel was not predicted properly by the EM model.

For Type 4, which has a large unheated rod at the central region and a ferrule-type spacer grid, the thermal load and the mass flux at the central region (INR3) were lower compared to those of the surrounding channels. In this case, the void outflow due to a void drift was more significant than the void inflow due to the equal volume exchange at the INR3 channel. A net outflow of a void can increase the mass flux at the INR3 channel, which in turn will reduce the channel enthalpy. The MATRA and MARS codes revealed good prediction accuracy for the steady-state void distribution for Type 4, as shown in Fig. 8.

The calculated void fractions for all of the subchannels in this benchmark exercise are compared with the measured data in Fig. 9. It was found that the void fraction correlation employed in the MATRA code tends to under-predict the cross-section averaged void fraction of the test bundle as the bundle exit quality increases. The two-fluid model used in the MARS code predicts the average void fraction for all the ranges of the qualities examined in this exercise reasonably well.

The statistics for the prediction accuracy as represented by the difference in the subchannel void fractions between the predicted and measured values (P-M) are summarized in Table 4. The analysis results achieved thus far indicate that the subchannel void distribution for a steady state condition can be predicted reasonably well by both the MATRA and the MARS codes with an appropriate modeling of the void drift phenomenon. The maximum and minimum deviations of the subchannel void fraction were observed for Type 0-3 and Type 4, respectively.

4.3 Transient Macroscopic Grade Void Distribution Benchmark

Transient experiments were performed to measure the cross-sectional averaged transient void fraction over a range of pressure, flow, and power variations. These are very important for the benchmark of the subchannel analysis codes in terms of a transient DNBR (Departure from Nucleate Boiling Ratio) prediction. A turbine trip transient without a bypass and a recirculation pump trip transient were simulated by employing the Type 4 test bundle with the boundary conditions in Fig. 3. The macroscopic grade void fractions calculated by the MATRA and MARS codes were compared with the transient test data measured by the DM #3 and the CT, which were located at the axial locations of 0.682 m and 3.758 m, respectively, above the bottom of the heated section.

For the analysis of this transient benchmark exercise, a constant void drift coefficient (K_{VD}=1.4) model was selected in the MATRA code because the flow-regime-dependent K_{VD} model revealed a convergence problem for the pump trip transient. The influence of the turbulent mixing model on the analysis results of the transients was examined by employing two different models (the EVVD model with K_{VD}=1.4 and the EM model). As a result, it was found that the macroscopic void fraction during the transients was mostly unaffected by the turbulent mixing model.

For the two transient cases, it was found that both the MATRA and the MARS codes predicted the overall behavior of the bundle cross-sectional averaged void fraction reasonably well, as can be seen in Fig. 10. It was observed that the MATRA code revealed a quick response near the fast transient period (approximately 12 seconds after the transient). This is due to the homogeneous mixture model of the MATRA code. On the other hand,

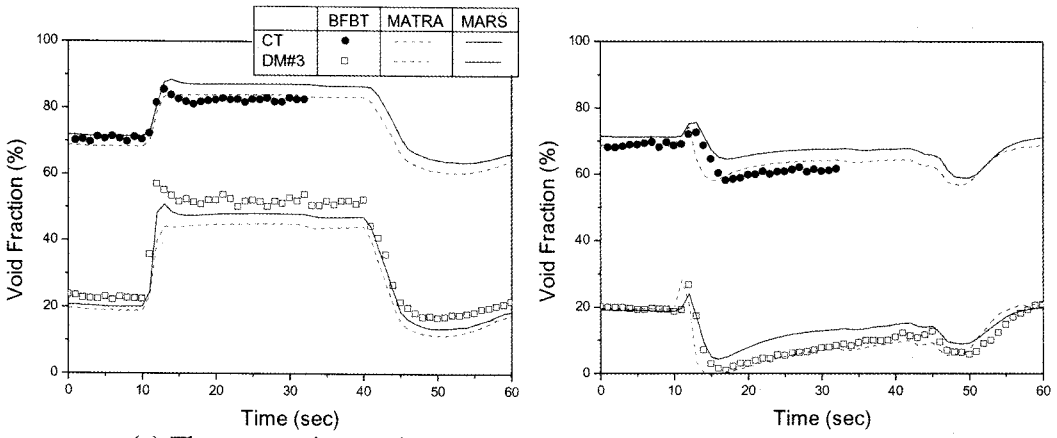

(a) The pump trip transient (b) The turbine trip transient

Fig. 10. Comparison of Macroscopic Void Fractions Under Transient Conditions

the MARS code revealed greater prediction accuracy during the fast transient period.

For these transient calculations, a personal computer with a Pentium IV CPU and a clock speed of 3.20 GHz was used. For a 60-second turbine trip transient calculation with a 1/2 radial symmetry model, the MARS code required nearly 4,560 seconds, whereas the MATRA code consumed only 519 seconds. This difference is mainly due to the performance of adopted numerical schemes. In the MARS calculation, the time step size was limited by the material Courant limit, which was approximately $3.1\text{x}10^{-3} \sim 6.2\text{x}10^{-3}$ seconds. In the MATRA calculation, a constant time step of 0.02 seconds was used throughout the transients owing to an implicit time scheme. It should be noted that the axial flow is assumed to be dominant in the MATRA code. These features allow for faster calculation of MATRA but do not guarantee a convergence when the transverse flow is strong. However, the MARS code is very robust in any case but with longer computation times.

5. CONCLUSIONS

The subchannel code MATRA and the system code MARS were examined with BFBT benchmark exercises that provided subchannel grade void fraction data. For steady-state subchannel void distribution problems, the mean error and standard deviation of the (P-M) were calculated as -1.2 % and 5.5 % for the MATRA code, and 0.6 % and 5.7 % for the MARS code, respectively. In addition, both codes revealed reasonable prediction capability for the two transient benchmark exercises.

For the benchmark exercises evaluated in this study, the MATRA code revealed reasonable accuracy with a pertinent computing time. However, it was also found that the existing void drift model incorporated into the MATRA code did not provide appropriate results, specifically for a cold channel with a high mass velocity. Moreover, the MARS code provided results that were more accurate for thermally non-equilibrium cases and fast transient conditions in spite of its relatively long computing time. Thus, it is recommended to make the best use of the complementary nature of the MATRA and MARS codes for the analysis of the thermal hydraulics in rod bundles.

ACKNOWLEDGEMENT

The authors are very grateful for the access to the OECD NUPEC BFBT Benchmark Program, through which the valuable experiment data for the code assessment was obtained. The authors thank Dr. Utsuno at NUPEC, Prof. Ivanov at Penn. State University, and Mr. Sartory at OECD for their efforts pertaining to the benchmark program. This work was performed as a part of the Nuclear Research and Development Program supported by the Ministry of Education, Science and Technology of the Republic of Korea.

NOMENCLATURE

A	Flow area
d_{hy}	Hydraulic diameter
f	Friction factor
f_T	Turbulent momentum factor
F	Volumetric force
g	Gravitational acceleration
G	Mass flux
G_{avg}	Average mass flux weighted by channel flow area, $G_{avg} = (G_iA_i+G_jA_j)/(A_i+A_j)$
h	Enthalpy
k	Thermal conductivity
K	Form loss factor
l	Channel center-to-center distance
K_{VD}	Void drift coefficient
$\dot{m}$	Mass flow rate

$\vec{M}_k^{\Gamma}$	Average supply of momentum to phase k due to mass transfer to phase k
$\vec{M}_k^{d}$	Average drag force and virtual mass force on phase k
P	Pressure
Q	Heat source
$\vec{Q}_k$	Average k-phase conduction vector
q''_{ik}	Volumetric interface heat transfer
$\vec{q}_k^{T}$	k-phase turbulent heat flux
s_{ij}	Channel gap
$\vec{T}_k$	Average phasic turbulent stress tensor
u	Velocity
v'	Effective specific volume, $v' = \sum_k (\chi_k^2/\rho_k\alpha_k)$
w_{ij}	Crossflow from channel-i to channel-j per unit axial length
z	Axial coordinate

Greek

α	Volumetric fraction or coefficient
β	Turbulent mixing coefficient
χ	Quality
ξ	Heated perimeter
ρ	Density
θ	Inclination angle or a two-phase multiplier
$\vec{\tau}_k$	Average k-phase viscous stress tensor
Γ	Volumetric vapor generation rate

Subscripts

avg	Average
e	Entrained liquid droplet phase
f	Liquid phase
ik	Interface to k-phase
k	phase (gas or liquid)
l	Continuous liquid phase
m	Two-phase mixture
v	Vapor or gas phase

Superscripts

*	Quantity at donor subchannel

REFERENCES

[1] C.W. Stewart, C.L. Wheeler, R.J. Cena, C.A. McMonagle, J.M. Cuta, and D.S. Trent "COBRA-IV: The Model and The Method," BNWL-2214, PNL (1977).

[2] J.E. Kelly, S.P. Kao, and M.S. Kazimi, "THERMIT-2: A Two-Fluid Model for Light Water Reactor Subchannel Transient Analysis," MIT-EL 81-014, MIT (1981).

[3] Y.J. Yoo, D.H. Hwang, and D.S. Sohn, "Development of A Subchannel Analysis Code MATRA Applicable to PWRs and ALWRs," *J. Korean Nuclear Society*, **31**, 314 (1999).

[4] D.H. Hwang, S.Y. Chun, K.K. Kim, and C.C. Lee, "Mass Velocity and Cold-wall Effects on Critical Heat Flux in an Advanced Light Water Reactor," *Nucl. Eng. Design*, **237**, 369 (2007).

[5] X. Cheng and D.H. Hwang, "Subchannel analysis of LBE-cooled fuel assemblies of Accelerator Driven Systems," *Proceedings of GLOBAL 2005*, Paper 115, Tsukuba, Japan, 2005.

[6] K.H. Han, K.W. Seo, D.H. Hwang, and S.H. Chang, "Development of a Thermal Hydraulic Analysis Code for Gas-cooled Reactors with Annular Fuels," *Nucl. Eng. Design*, **236**, 164 (2006).

[7] D.H. Hwang, K.W. Seo, and H. Kwon, "Assessment of Critical Heat Flux Data Base for Rod Bundles," *Proceeding of KNS Spring Meeting*, Kyeongju, Korea, 2008.

[8] J.J. Jeong, K.S. Ha, B.D.Chung, and W.J. Lee, "Development of A Multi-dimensional Thermal-Hydraulic System Code, MARS 1.3.1," *Annals of Nuclear Energy*, **26**, 1611 (1999).

[9] M.J. Thurgood, J.M. Kelly, T.E. Guidotti, R.J. Kohrt, and K.R. Crowell, "COBRA/TRAC - A Thermal-Hydraulic Code for Transient Analysis of Nuclear Reactor Vessels and Primary Coolant Systems," NUREG-CR-3046, U.S. Nuclear Regulatory Commission (1983).

[10] J.J. Jeong, D.H. Hwang, and B.D. Chung, "Improvement of the Subchannel Flow Mixing Model of the MARS Code," *Nuclear Technology*, **156**, 360 (2006).

[11] H. Herkenrath, W. Hufschmidt, U. Jung, and F. Weckermann, Experimental Investigation of The Enthalpy and Mass Flow Distribution in 16-Rod Clusters with BWR-PWR-Geometries and Conditions, EUR 7575 EN, ISPRA (1981).

[12] R.T. Lahey, Jr., B.S. Shiralkar, and D.W. Radcliffe, Two-Phase Flow and Heat Transfer in Multi-rod Geometries: Subchannel and Pressure Drop Measurements in a Nine-Rod Bundle for Diabatic and Adiabatic Conditions, GEAP-13049, GE (1970).

[13] A. Tapucu, M. Geckinli, N. Troche, and R. Girard, "Experimental Investigation of Mass Exchanges Between Two Laterally Interconnected Two-Phase Flows," *Nucl. Eng. Design*, **105**, 295 (1998).

[14] B. Neykov, F. Aydogan, L. Hochreiter, K. Ivanov, H. Utsuno, K. Fumio, E. Sartori, and M. Martin, NUPEC BWR Full-Size Fine-Mesh Bundle Test Benchmark, Volume I. Specifications, NEA/NSC/DOC(2005)5, OECD Nuclear Energy Agency (2005).

[15] R.T. Lahey, Jr., and F.J. Moody, *The Thermal Hydraulics of a Boiling Water Reactor*, 2nd Ed., ANS, La Grange Park, Illinois USA, p. 122 (1977).

[16] J.J. Jeong, W.J. Lee, and B.D. Chung, "Simulation of A Main Steam Line Break Accident Using A Coupled 'System Thermal-Hydraulics, Three-dimensional Reactor Kinetics, and Hot Channel' Analysis Code," *Annals of Nuclear Energy*, **33**, 820 (2006).

[17] J.M. Gonzalez-Santalo and P. Griffith, "Two-phase flow Mixing in Rod Bundle Subchannels," ASME Paper 72-WA/NE-19 (1972).

[18] D.H. Hwang, Y.J. Yoo, W.K. In, and S.Q. Zee, "Assessment of the Interchannel Mixing Model with a Subchannel Analysis Code for BWR and PWR Conditions," *Nucl. Eng. Design*, **199**, 257 (2000).

[19] J.E. Kelly, Development of a Two-Fluid, Two-Phase Model for Light Water Reactor Subchannel Analysis, PhD Thesis, Department of Nuclear Engineering, MIT (1980).

[20] S.G. Beus, A Two-phase Turbulent Mixing Model for Flow in Rod Bundles, Westinghouse Report, Bettis Atomic Power Laboratory, WAPD-T-2438 (1971).